Harvesting body heat through clay-based ionic thermoelectric devices

Parijat Pratim Das[a], Raktim Gogoi[a*], Sanjay Biswas[a], Tirthanav Das[a] and Kalyan Raidongia,[a,b*]

[a]*Department of Chemistry, Indian Institute of Technology Guwahati, Guwahati, Assam 781039, India.*

[b]*Centre for Nanotechnology, Indian Institute of Technology-Guwahati, Kamrup, Assam 781039, India*

E-mail: g.raktim@iitg.ac.in, k.raidongia@iitg.ac.in

Contents

1.Experimental Section:

1.1. Materials required:

Montmorillonite clay, Carbon nanotube was purchased from Sigma Aldrich, Sodium Chloride (NaCl), Lithium Chloride (LiCl), Sodium dodecyl sulfate (SDS), Hydrochloric acid (HCl) and Nitric acid (HNO_3) was purchased from Sisco Research Laboratories Pvt. Ltd., Conductive Silver Paste were purchased from Alfa Aesar, PTFE membrane, Copper (Cu) electrodes were purchased from local market.

1.2. Exfoliation of Montmorillonite clay and membrane preparation

Bulk MMT particles were exfoliated using a two-step ion exchange method. In the first step, 500 mg of MMT clay was refluxed in an aqueous solution of saturated sodium chloride for 48 hrs, followed by washing with distilled water. In the second step, sodium-exchanged MMT was refluxed in an aqueous solution of lithium chloride (2M) for 24 hrs, followed by washing with DI water several times. After the washing the Li^+ exchanged MMT was characterized and used for the preparation of MMT membrane.

Freestanding MMT membranes were prepared through vacuum filtration of aqueous dispersions of MMT nanosheets (~ 15 mL, 10 mg mL^{-1}) using a PTFE membrane with a pore diameter of 100 nm. Subsequently, the membrane was dried at 45 ºC and the freestanding membrane was peeled off from the PTFE membrane.

1.3. Preparation of oxidised multi-walled Carbon nanotubes

Multi-walled carbon nanotubes (MWCNTs) were treated with a diluted nitric acid (HNO_3) solution under reflux conditions at 120 °C in a 200 mL round-bottom flask for 3 hours to induce surface oxidation. The residual acid was removed by washing with DI water. The oxidized MWCNTs were then dispersed in DI water. To enhance the stability of MWCNT dispersion, sodium dodecyl sulfate (SDS) was introduced as a surfactant. The mixture was subsequently subjected to probe sonication for 2 hours to achieve uniform dispersion[1].

1.4. Ionic thermoelectric device fabrication

Freestanding MMT membranes were cut into rectangular strips of size 2 cm × 0.8 cm × 0.008 cm, and copper wires were attached to both ends of the membrane as electrodes using conductive silver paste. The MMT membrane were then attached to the glass slide with adhesive tape for the thermoelectric studies.

The MMT-i-TE device was positioned on top of two Peltier modules, such that upon application of DC voltage, one side of the Peltier modules becomes hotter and the other side becomes cooler, creating a temperature gradient. The Testo 735 temperature sensing instrument, equipped with two K-type thermocouples, was fixed at both ends of the membrane to monitor the temperature gradient. The voltage and current output of the MMT-i-TE device were recorded using a digital source meter measurement unit (Keithley Source Meter 2450).

1.5. Nanofluidic device fabrication

To construct MMT membrane-based nanofluidic devices, MMT membranes were precisely cut into rectangular segments and immersed in a mixture of PDMS prepolymer and curing agent. After curing the polymer, two reservoirs were created in the PDMS structure to expose both ends of the membrane, enabling soaking of MMT channels with deionized water (DI) and electrolyte solutions. Before nanofluidic studies, the membranes were hydrated through the reservoirs by soaking it in DI water for 12 hours. Subsequently, hydrochloric acid (HCl) solutions with concentrations ranging from 10^{-6} to 1 M were introduced into the reservoirs and left to equilibrate for approximately 6 hours before conducting current-voltage (*I-V*) measurements.

2. Characterizations:

Surface morphology was characterized by field emission scanning electron microscopy (FESEM, Zeiss Sigma), atomic force microscopy (AFM, Oxford Cypher), and field emission transmission electron microscopy (FETEM, JEOL 2100F). Infrared spectra were recorded using a PerkinElmer Spectrum Two spectrometer. Thermal stability was evaluated by thermogravimetric analysis (TGA, Netzsch STA449F3A00). ζ-Potential measurements of aqueous nanosheet dispersions and other samples were performed using a Zetasizer (Malvern Nano-ZS90). X-ray diffraction (XRD) patterns were obtained with a Bruker D-205505 diffractometer using Cu-Kα radiation (λ = 1.5406 Å). Electrical measurements were conducted using a Keithley 2450 SourceMeter.

3. Supplementary Results:

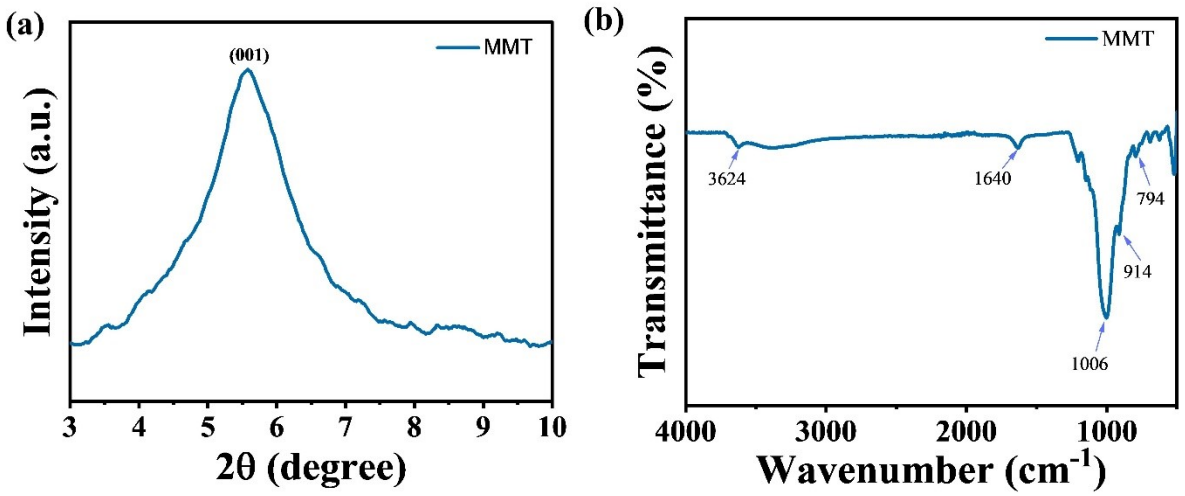

Figure S1: (a) p-XRD pattern of exfoliated MMT clay and b) FTIR spectra of MMT membrane.

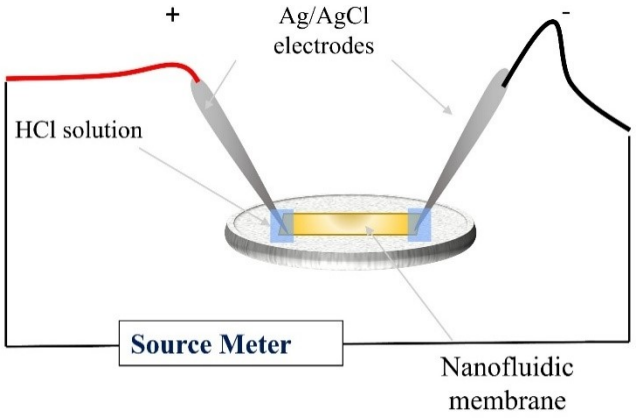

Figure S2: Schematic illustration of the nanofluidic device.

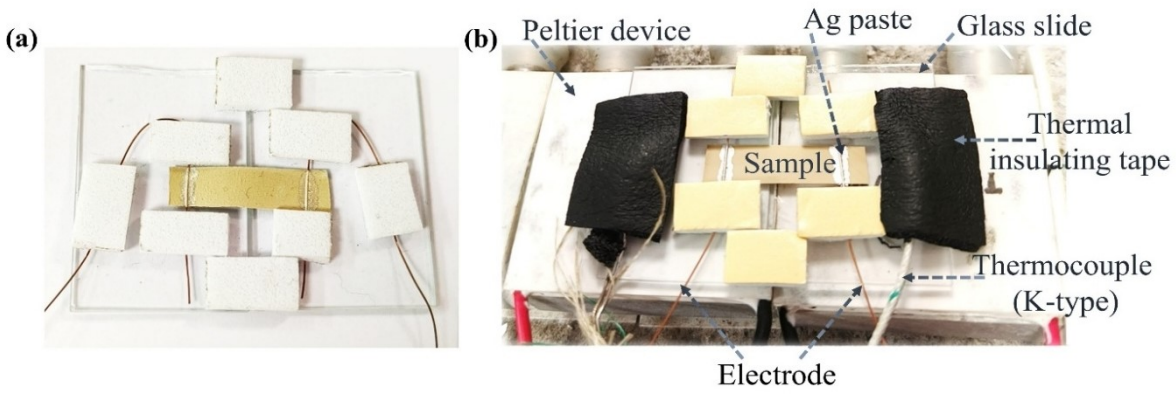

Figure S3: (a) and (b) Digital photograph of i-TE device.

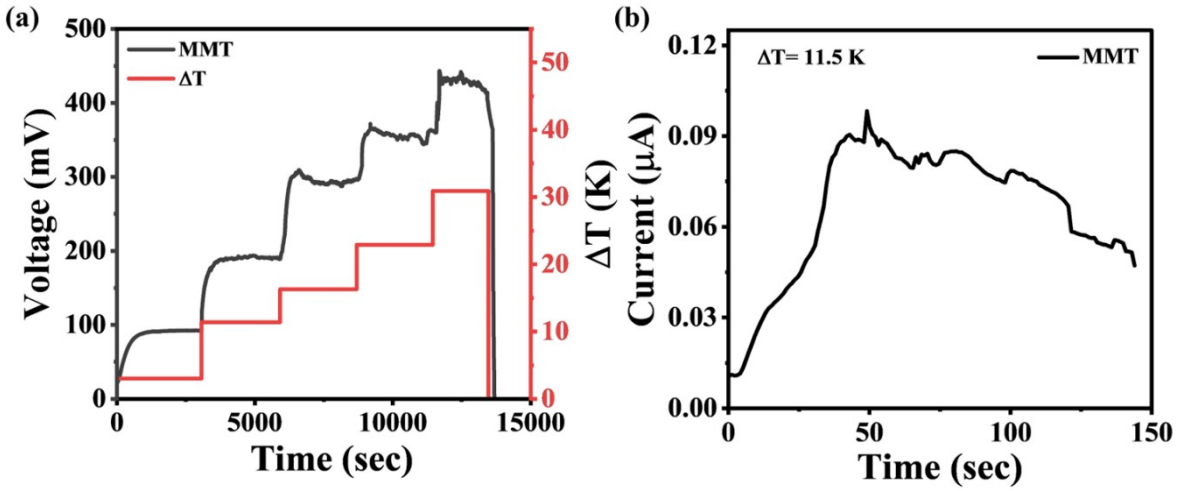

Figure S4: (a) Generation of thermovoltage at different temperature gradient for MMT membrane. (b) Generation of current under ΔT of 11.5 K.

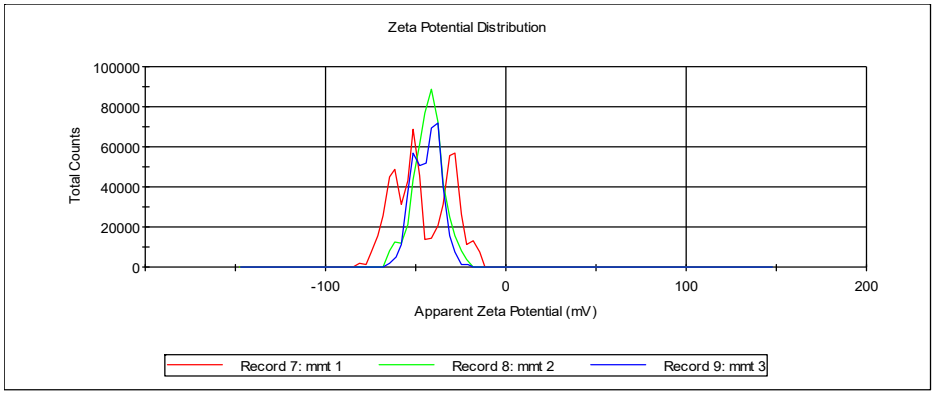

Figure S5: Zeta potential distribution curve of aqueous dispersion of MMT nanosheets. The average zeta potential is found to be -44.4 ± 1.72 mV.

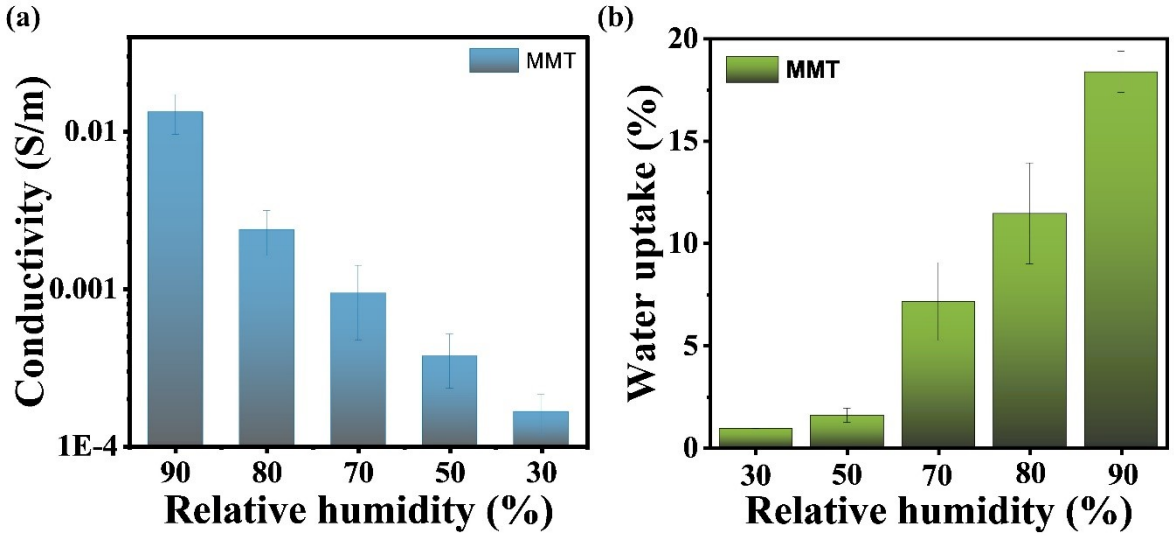

Figure S6: (a) Ionic conductivity value of MMT membrane at different relative humidity. (b)The concordant increment of water uptake capacity of MMT membrane with increasing relative humidity (RH %).

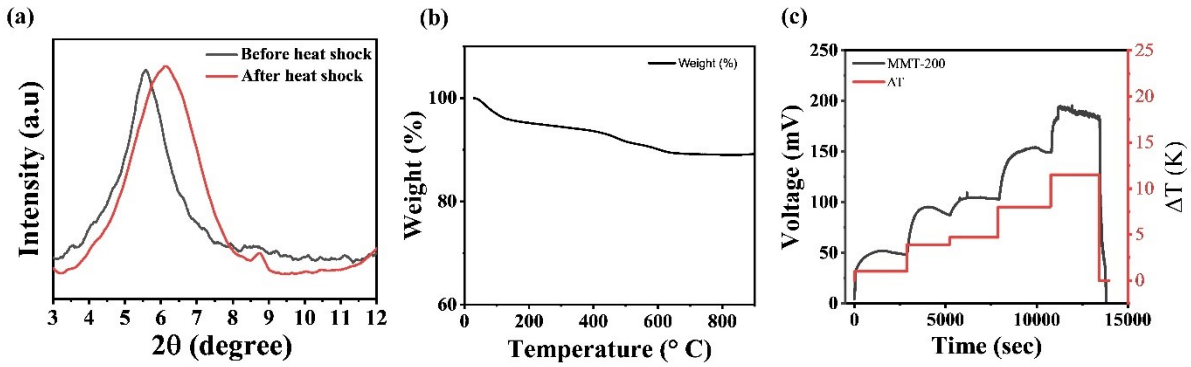

Figure S7: (a) p-XRD pattern of MMT membrane before and after heat shock. (b) TGA plot for exfoliated MMT clay. (c) Thermovoltages generated at different temperature gradient after thermal treatment at 200 °C (MMT-200).

Figure S7(a) shows the pXRD patterns before and after the heat treatment, revealing a shift in the (*001*) peak position. This shift is likely due to a reduction in interlayer spacing caused by the loss of loosely bound water molecules.

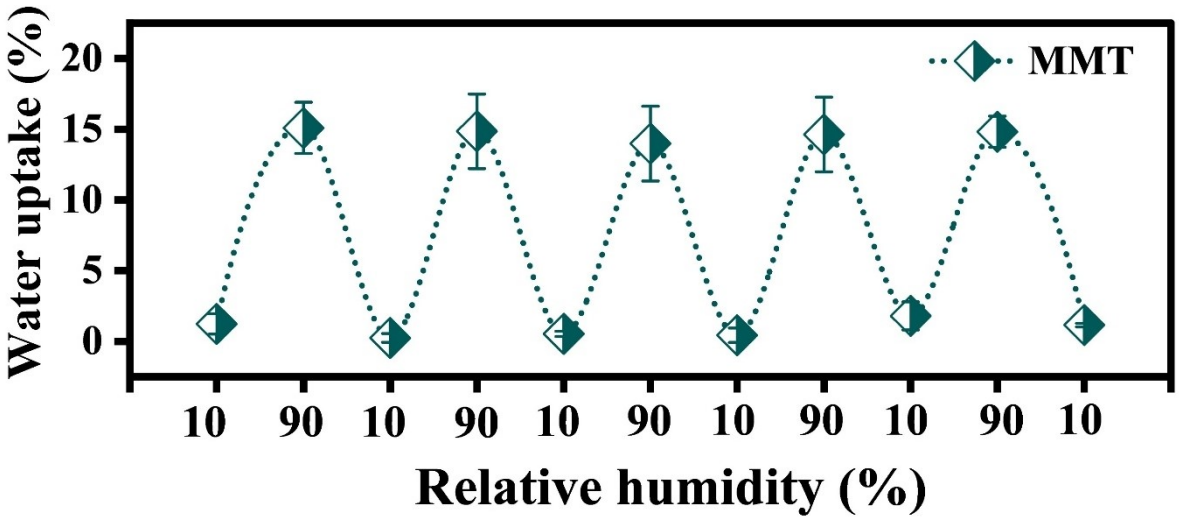

Figure S8: Reversible dehydration-rehydration behaviour of the MMT membrane during alternating low (10% RH) and high-humidity (90% RH) cycles.

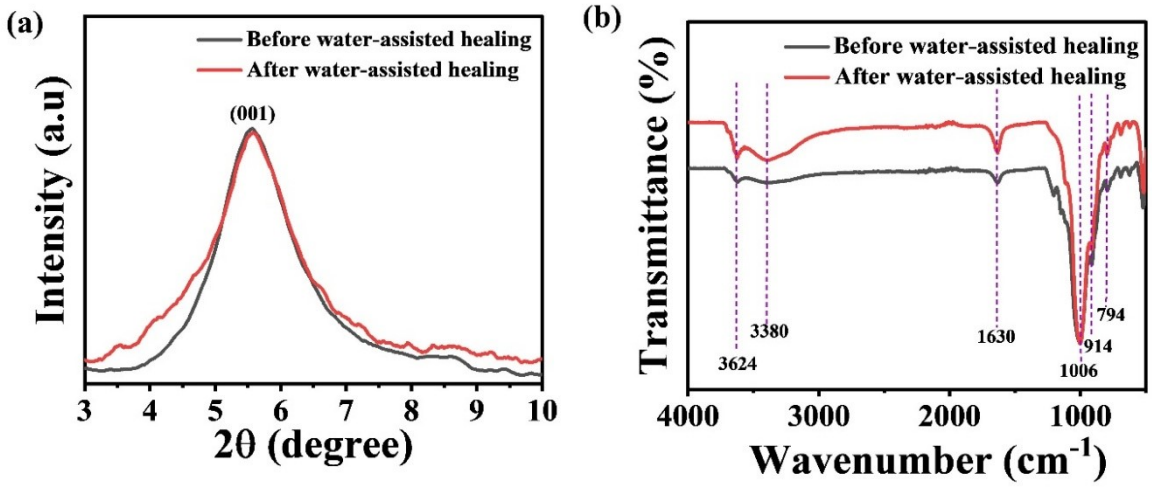

Figure S9: (a) p-XRD pattern MMT membrane before and after water assisted healing. (b) Comparative FTIR spectra of MMT membrane before and after water assisted healing (RH %).

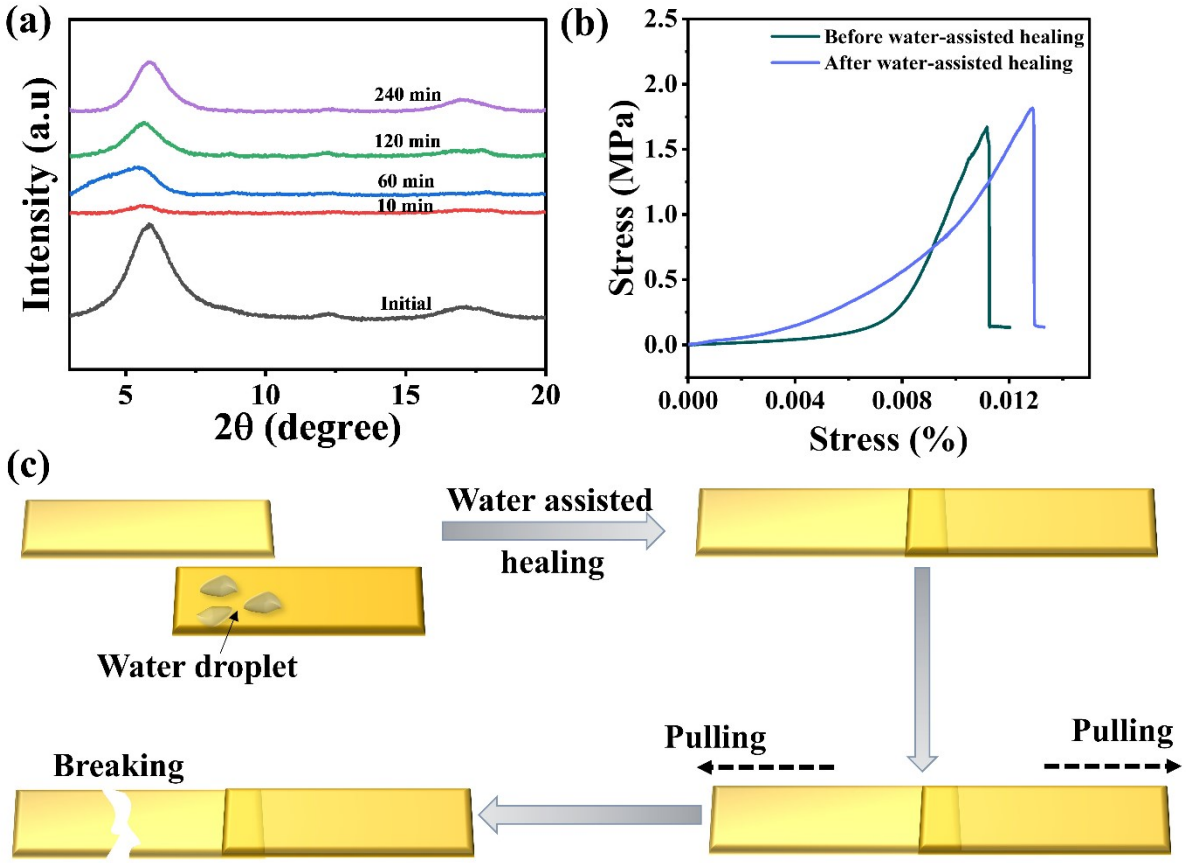

Figure S10: (a) *In situ* XRD patterns of the MMT membrane recorded at different time intervals after introducing a water droplet onto its surface. **(b)** Comparison of the mechanical strength of the MMT membrane before and after the water-assisted healing process. **(c)** Schematic illustration showing the fabrication process of the MMT device used for mechanical property measurements.

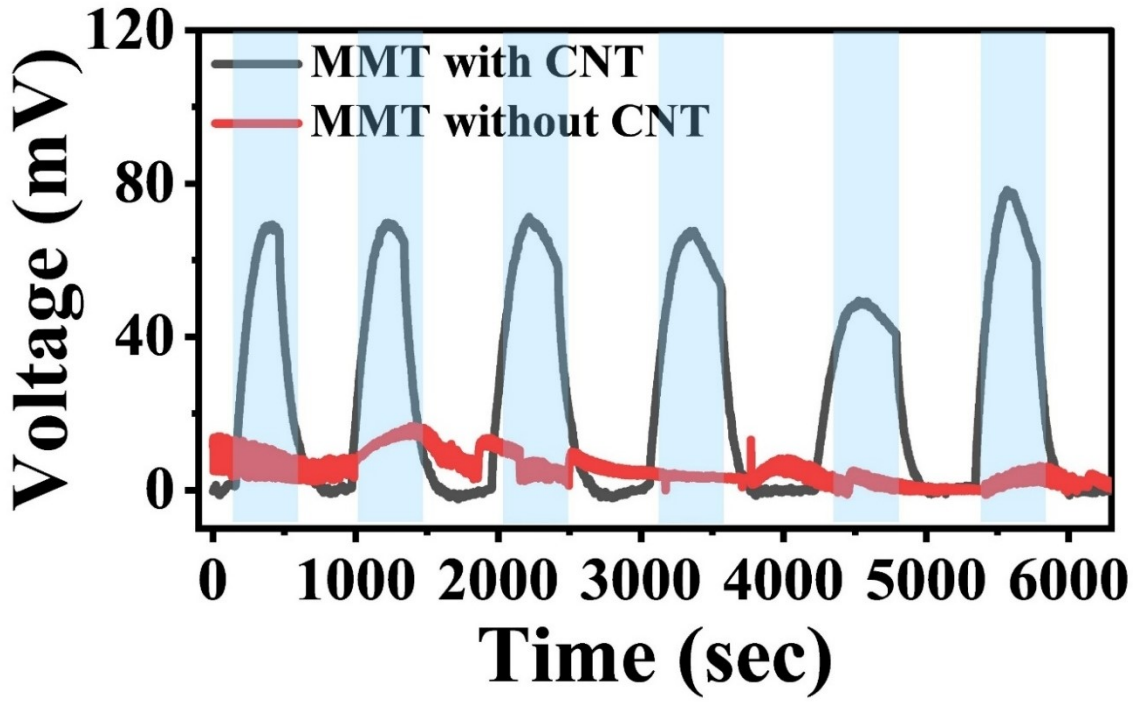

Figure S11: Thermovoltage response of the MMT membrane with and without CNTs under light illumination.

Figure S11 shows the thermovoltage response of the MMT membrane without CNTs. The poor thermovoltage yielded a highly fluctuating curve, attributed to the poor light absorption and low thermal conductivity of MMT. As MMT failed to create a sufficient temperature gradient under illumination, ion movement and thermovoltage generation were negligible. In contrast, the incorporation of CNTs towards one side of the MMT membrane significantly enhances the photothermal performance, as CNTs efficiently absorb light and convert it into heat. This leads to a stable temperature gradient and promotes directional ion diffusion within the MMT channels, resulting in an improved and stable thermoelectric output. Importantly, CNTs did not modify the intrinsic thermoelectric parameters of MMT. Instead, CNTs drop-cast on one end

of the MMT membrane absorbed light and generate a ΔT between coated and uncoated region of the MMT membrane, which led to the photothermoelectric voltage output.

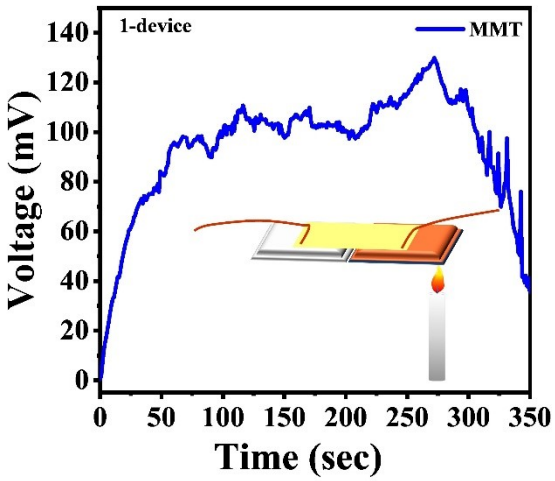

Figure S12: Thermoelectric voltage generated upon direct exposure of the i-TE device to an open flame (inset: schematic diagram of the experimental setup).

4. Comparison table:

Table 1: Comparative summary of the Seebeck coefficient (S_i), ionic conductivity (σ_i), and power factor, PF of the MMT membrane with previously reported polymer- and hydrogel-based ionic thermoelectric (i-TE) materials.

Materials	**Seebeck coefficient, S_i (mV K^{-1})**	**Ionic conductivity, σ_i (S m^{-1})**	**Power factor, PF (mW m^{-1} K^{-2})**	**Reference**
Ionogel	22.9	1.75	0.87026	[2]
Ionogel	11.55	7.9	0.46014	[3]

Ionogel	26.1	0.67	0.455	[4]
Ionogel	43.8 ± 1.0	1.94	3.72	[5]
Ionogel	34.5	0.84	0.9998	[6]
Hybrid ionogel flim	47.5	4.37	9.8458	[7]
Hydrogel	13	22.64	3.831	[8]
Hydrogel	7.48	3.99	0.2235	[9]
Hydrogel	-20.65	0.062	0.26438	[10]
Hydrogel	3.26	0.045	0.00048	[11]
Hydrogel	2.96	3.651	0.032	[12]
Gels	14.8	4.75	1.0404	[13]
Gels	41.8	0.0182	0.0318	[14]
Ionic TE hybrid materials	8.1	25.6	1.6	[15]
Organic-inorganic hybrid polymer	17.90 ± 0.78	0.187 ± 0.068	5.99 ± 0.57	[16]
Polymer composite membrane	-26.25	0.847	0.584	[17]
Polymer hybrid materials	1.2	0.8	0.00115	[18]
Polymeric ionic gel	5.84 (p-type) and -4.18 (n-type)	0.041 (p-type) and 0.027 (n-type)	0.00059 (p-type) and 0.00139 (n-type)	[19]
Two dimensional nanosheet membrane	26.3 ± 0.7	0.57	-	[20]
Two dimensional nanosheet membrane	−13.7 ± 0.2 (n-type) 12 ± 1.9 (p-type)	0.49	0.09 ± 0.005	[21]

Clay based	14.4 ± 0.4	0.31	-	[22]	
This work	13.63 ± 1.13	0.01336 ± 0.00379	0.00248 ±0.00081		

5. References:

1 B. Saikia, M. Dey, P. Garg, R. Gogoi, R. Manik and K. Raidongia, *Chem. Eng. J.*, 2024, **497**, 154840.

2 M. Li, H. Xu, M. Luo, X. Qing, W. Wang, W. Zhong, Q. Liu, Y. Wang, L. Yang, X. Zhu and D. Wang, *Chem. Eng. J.*, 2024, **485**, 149784.

3 G. Fan, K. Liu, H. Su, Y. Luo, Y. Geng, L. Chen, B. Wang, Z. Mao, X. Sui and X. Feng, *Chem. Eng. J.*, 2022, **434**, 134702.

4 H. Cheng, X. He, Z. Fan and J. Ouyang, *Adv. Energy Mater.*, 2019, **9**, 1901085.

5 Z. Liu, H. Cheng, Q. Le, R. Chen, J. Li and J. Ouyang, 2022, **2200858**, 1–8.

6 Y. Fang, H. Cheng, H. He, S. Wang, J. Li, S. Yue, L. Zhang, Z. Du and J. Ouyang, 2020, **2004699**, 1–8.

7 M. Li, R. Jing, K. Jia, H. Xu, M. Luo, X. Zhu, X. Qing, W. Wang, W. Zhong, L. Yang and D. Wang, *Adv. Funct. Mater.*, 2025, **35**, 2415856.

8 M. Muddasar, N. Menéndez, Á. Quero, M. A. Nasiri, A. Cantarero, J. García-Cañadas, C. M. Gómez, M. N. Collins and M. Culebras, *Adv. Compos. Hybrid Mater.*, 2024, **7**, 47.

9 N. Jabeen, C. M. Gómez, R. Muñoz-Espí, A. Cantarero, M. N. Collins and M. Culebras, *Green Chem.*, 2025, **27**, 8283–8299.

10 L. Chen, X. Rong, Z. Liu, Q. Ding, X. Li, Y. Jiang, W. Han and J. Lou, *Chem. Eng. J.*, 2024, **481**, 148797.

11 M. Fu, Z. Sun, X. Liu, Z. Huang, G. Luan and Y. Chen, 2023, **2306086**, 1–11.

12 W. Qian, S. Jia, P. Yu, K. Li, M. Li, J. Lan, Y.-H. Lin and X. Yang, *Mater. Today Phys.*, 2024, **49**, 101589.

13 X. He, H. Cheng, S. Yue and J. Ouyang, *J. Mater. Chem. A*, 2020, **8**, 10813–10821.

14 Q. Li, D. Yu, S. Wang, X. Zhang, Y. Li and S. Feng, 2023, **2305835**, 1–8.

15 Z. A. Akbar, J. W. Jeon and S. Y. Jang, *Energy Environ. Sci.*, 2020, **13**, 2915–2923.

16 Y. T. Malik, Z. A. Akbar, J. Y. Seo, S. Cho, S.-Y. Jang and J.-W. Jeon, *Adv. Energy Mater.*, 2022, **12**, 2103070.

17 B. Chen, J. Feng, Q. Chen, S. Xiao, J. Yang, X. Zhang, Z. Li and T. Wang, *npj Flex. Electron.*, 2022, **6**, 79.

18 N. Pereira, L. Afonso, M. Salado, C. R. Tubio, D. M. Correia, C. M. Costa and S. Lanceros-mendez, 2024, **2400041**, 1–9.

19 S. Kim, M. Ham, J. Lee, J. Kim, H. Lee and T. Park, 2023, **2305499**, 1–11.

20 R. Gogoi, H. Madeshwaran, A. Ghosh, Y. Green and K. Raidongia, *Adv. Funct. Mater.*, 2023, **33**, 2301178.

21 R. Gogoi, A. Ghosh, P. Deka, K. K. R. Datta and K. Raidongia, *Mater. Horizons*, 2023, **10**, 3072–3081.

22 R. Gogoi, H. Madeshwaran, P. Pratim Das, P. Garg, N. Nath, B. Saikia and K. Raidongia, *Chem. Eng. J.*, 2024, **487**, 150440.